Quantum Electronics **47** (9) 783–789 (2017)

https://doi.org/10.1070/QEL16467

Optimal periodic frequency combs for high-efficiency optical quantum memory based on rare-earth ion crystals

N.M. Arslanov, S.A. Moiseev

Abstract. **The possibility of enhancing the quantum efficiency of photon echo broadband quantum memory in rare-earth-ion-doped crystals with a frequency comb structure of optical transition inhomogeneous broadening is studied. We have found the optimal parameters of the frequency combs for implementing the preassigned quantum efficiency in the chosen spectral range of the optical transitions of rare-earth ions with real parameters. The obtained results allow the conditions to be formulated for increasing the efficiency of broadband quantum memory. The possibilities of experimental implementation of such memory are also discussed.**

Keywords: *photon echo broadband quantum memory, quantum efficiency, optically dense media, inorganic crystals with rare-earth ions, quantum repeater.*

1. Introduction

The effects of spin and photon echo [1, 2] have been actively developed in the experimental quantum informatics during the recent decade. In particular, new photon echo schemes in optically dense media with a time-reversible echo signal [3, 4] are being intensely studied for implementing the multiqubit quantum memory [5–9], which is necessary for constructing quantum repeaters [10] and a universal quantum computer [11]. Using a scheme [3] referred to as the CRIB (controlled reversible inhomogeneous broadening) protocol [12–14], a number of the protocol modifications have been proposed, differing in the implementation of atomic coherence dephasing, such as AFC (atomic frequency comb) [15, 16], GEM (gradient echo memory) [17–19], ROSE (revival of silenced echo) [20, 21], HYPER (hybrid photon echo rephrasing) [22], etc. These protocols significantly extended the possibilities of implementing the quantum memory based on the photon echo, including that in the microwave frequency range [23, 24]. The simplified scheme of the AFC protocol with parallel propagation of all light pulses used in the experimental studies allowed its potentialities for conserving the broadband quantum states of light and prospects of using it in the design of optical quantum repeater to be convincingly demonstrated [9].

In the experimental implementation of the AFC protocol, high expectations are generated by the use of rare-earth ions in inorganic crystals as quantum-information carriers. In such crystals, it became possible to conserve not only nanosecond light pulses, but also pico- and femtosecond ones, which caused the growing interest to these studies. The experiments with the AFC protocol in the $Pr:Y_2SiO_5$ crystal with the inhomogeneously broadened optical transition line $\Delta_{in} \approx 100$ GHz demonstrated the possibility of conserving single-photon wave packets with a duration of 100 ps [25]. In Ref. [8] a $Ti:Tm:LiNbO_3$ crystal with even greater inhomogeneous broadening $\Delta_{in} = 300$ GHz [26] was used. In Refs [8, 25] the accuracy of reconstruction of single-photon field states exceeded 90%. In such crystals the possibility of sequential writing and reading of 64 extremely weak light pulses (with a mean number of photons in a pulse $\bar{n} = 0.5$ [5]) and even 1060 light pulses [6] was demonstrated. We would also like to mention the demonstration of conserving the photon entangled states [25] and the time-bin qubits in 26 multiplexed spectral modes [8]. Recently the AFC protocol has been successfully used for operating with multifrequency recording channels [9].

Despite the mentioned great success, the quantum efficiency achieved in the experiments on observing the light echo in the direct scheme of the AFC protocol (the parallel propagation geometry of the light fields) amounted to only 35% [27–29], the maximal possible value being 54%. Placing atoms in an optical resonator allowed an increase in quantum efficiency to 58% [30, 31]. However, the application of resonators with a high Q-factor limits the operating spectral range. Therefore, the implementation of broadband high-efficiency quantum memory implies the use of the backward AFC protocol scheme without a resonator. In this scheme, the reconstructed signal propagates in the opposite direction with respect to the signal radiation, and according to the CRIB protocol [3] it is possible to achieve the quantum efficiency close to 100%.

In Ref. [32] it was found that the AFC protocol [15] does not allow one to achieve a high quantum efficiency for light fields having a spectral width comparable with that of the AFC structure because of the negative influence of dispersion effects, in contrast to protocols of CRIB [12] and GEM [19] type, where no such influence is observed. Note that the cause of this effect is fundamental and related to the absence of rigorous time reversibility of the light echo signal with respect to the process of signal light field absorption, in contrast to, e.g.,

N.M. Arslanov, S.A. Moiseev Kazan Quantum Centre, A.N. Tupolev Kazan National Research Technical University, ul. K. Marksa 10, 420111 Kazan, Russia; e-mail: s.a.moiseev@kazanqc.org, narkis@yandex.ru

Received 7 July 2017
Kvantovaya Elektronika **47** (9) 783–789 (2017)
Translated by V.L. Derbov

the initial CRIB protocol [3], where such reversibility takes place for an arbitrary spectral width of light signals [12–14]. Developing the approach [32] in the present paper, we propose particular ways of suppressing the spectral dispersion in the AFC structure of an optical transition with the real parameters of the optical transitions in the rare-earth ions in inorganic crystals taken into account. The optimal parameters of the modified AFC (MAFC) scheme that possesses a zero dispersion in a broad spectral range are found, which allow a high quantum efficiency for storing short light pulses to be achieved. Finally, the possibilities of experimental implementation of the approach are discussed.

2. Effect of the optical density on the spectral quantum efficiency

The AFC protocol makes use of resonance systems with inhomogeneous broadening Δ_{in} having the form of a discrete periodic sequence $\delta_j = n_j\Delta$ of narrow peaks having the width $\gamma \ll \Delta$, where $n_j = 0, \pm 1, \pm 2,...$ is an integer [15, 16]; and Δ is the separation between the adjacent spectral lines (Fig. 1). Note that for the first time such inhomogeneous broadening for the echo phenomenon was considered by Dubetskii and Chebotaev [33, 34]. They demonstrated the effect experimentally in a system of coupled pendulums. At present, the AFC structure in crystals with rare-earth ions is experimentally created by optical dip burning in the inhomogeneously broadened line of an optical transition in the used ions. After the fabrication of such a frequency comb, the signal light pulses are sent into the medium that excite long-lived atomic polarisation $P(t)$, experiencing fast dephasing due to the inhomogeneous line broadening. The excited polarisation is then recovered after the time $\tau = 2\pi/\Delta$, generating a light echo signal. Such automatic restoration is convenient in practice as compared to other protocols, in which it is necessary to use additional laser fields acting on the system of atoms or ions to reconstruct the dephased polarisation. For the quantum efficiency in the backward AFC protocol scheme, use is often made of the formula [16]

$$\eta \approx [1 - \exp(-\alpha L)]^2 \exp(-7/f^2). \quad (1)$$

Here $\alpha = \alpha_0/f$; $\alpha_0 L$ is the initial optical density of the resonance transition, at which the AFC structure is created; L is the sample length; and $f = \Delta/\gamma$ is the finesse (spectral sharpness) of the AFC structure of lines.

Note that in particular, the quantum efficiency η tends to 0.9 at $\alpha_0 L = 40$ and $f = 10$ [14]. According to Eqn (1), the efficiency η depends only on the averaged optical density αL and the finesse f, which also agrees with the experimental data, obtained for the direct AFC protocol in media with a minor optical density, where the quantum efficiency is low [27–29]. Figure 2 presents the map of the quantum efficiency η for the centre frequency of the optical transition versus the optical density $\alpha_0 L$ and the finesse f when the spectral width of the conserved pulse is small compared to the width of the AFC structure. As seen from Fig. 2a, in the existing experimental studies the crystals were used that allow the efficiency not exceeding 70%. To achieve $\eta > 90\%$, it is necessary to have a greater optical density of the AFC structure ($\alpha_0 L > 50$) and sufficient finesse ($f > 7$) (see Fig. 2b).

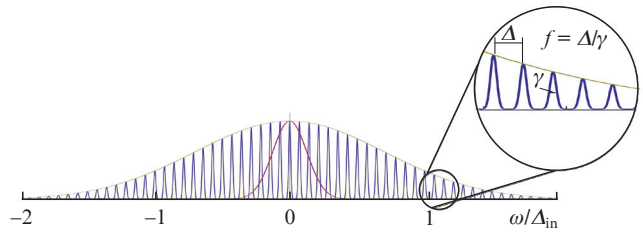

Figure 1. Spectral AFC structure of inhomogeneous line broadening and the spectrum of signal radiation in the line centre: Δ_{in} is the total line width; γ is the width of an individual peak; Δ is the separation between the adjacent peaks; and $f = \Delta/\gamma$ is the finesse.

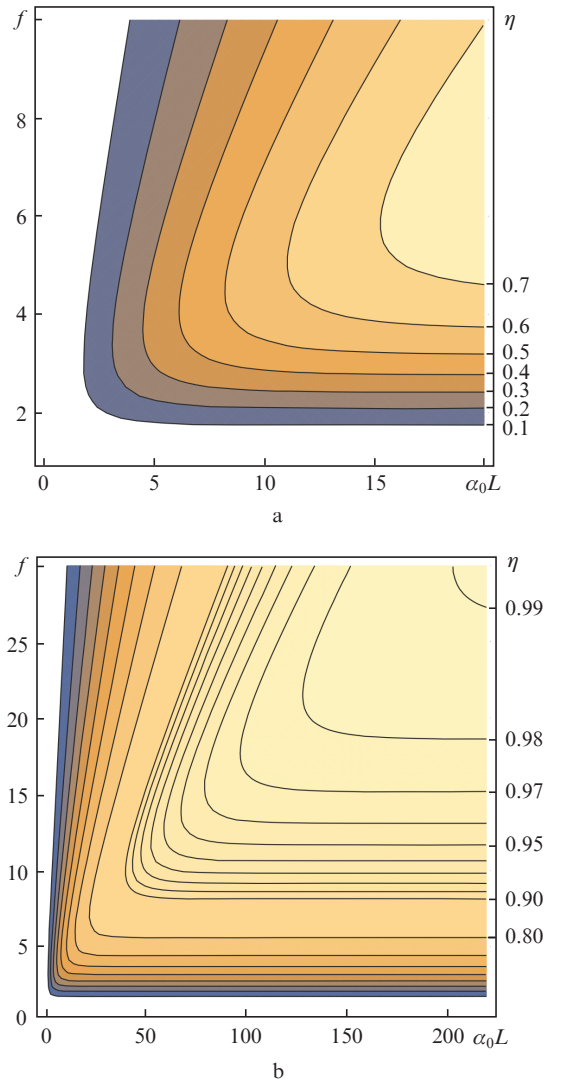

Figure 2. Map of quantum efficiency η at a zero frequency in the line centre. Black lines denote efficiency isolines for the efficiency values (a) from $\eta = 0.1$ to $\eta = 0.7$ with the step 0.1 and (b) from $\eta = 0.9$ to $\eta = 0.99$ with the step 0.01.

The efficiency of the signal field restoration is well described by formula (1) if the spectral width of the signal radiation is negligibly small compared to the spectral width of the AFC comb, Δ_{in} (Fig. 3) [32]. In the case of light fields with a large spectral width, the efficiency of restoration is noticeably decreased due to the violation of phase matching in the process of the echo signal emission (Fig. 4). The violation of

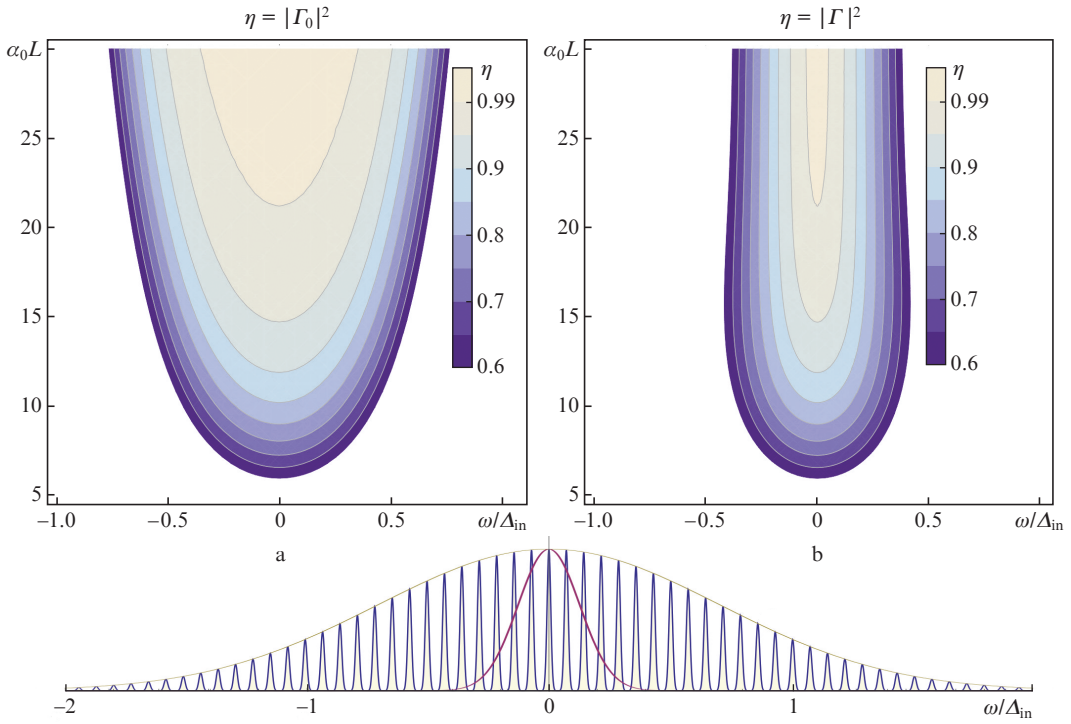

Figure 3. Spectral quantum efficiency $\eta(\omega)$ in the case of AFC structure formation in the entire inhomogeneously broadened line as a function of optical density of the resonance transition $\alpha_0 L$ (a) without and (b) with spectral dispersion taken into account.

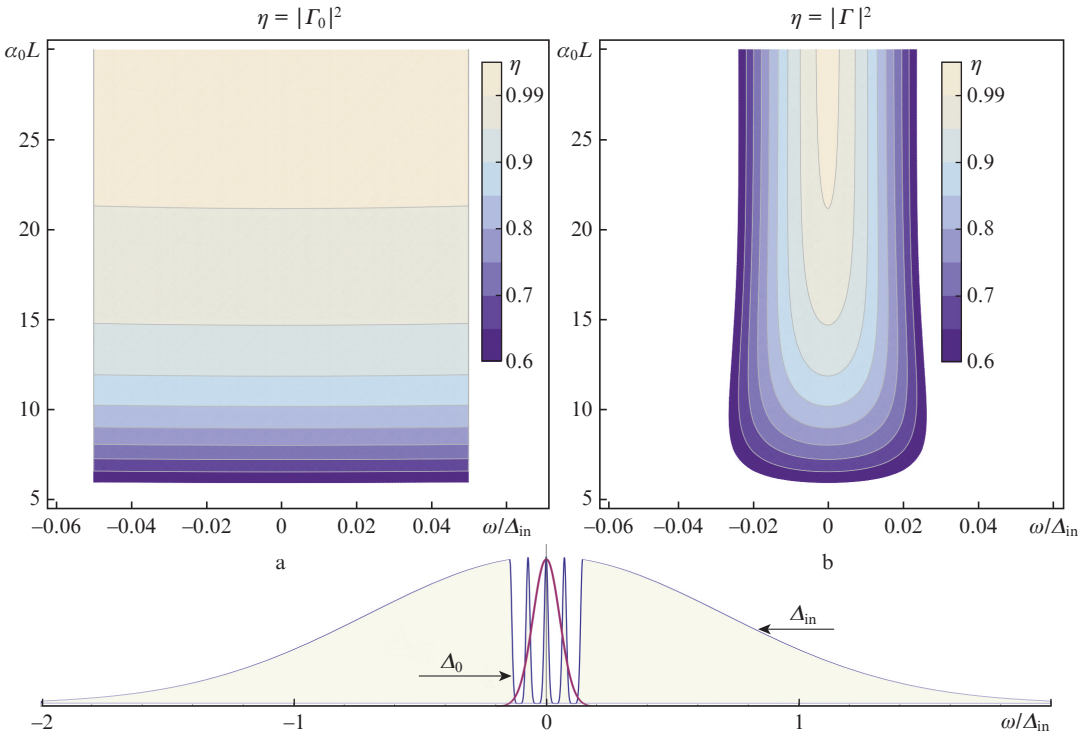

Figure 4. Spectral quantum efficiency $\eta(\omega)$ within the AFC structure with $\Delta_0 = 0.1\Delta_{in}$, formed in the narrow part of the inhomogeneously broadened line, as a function of resonance transition optical density $\alpha_0 L$ in the case (a) when the efficiency $\eta = |\Gamma_0|^2 = (1 - \exp(-\alpha L))^2$ (the influence of dispersion effects is not taken into account) and (b) when the efficiency η is described by the expression $\eta = |\Gamma(\omega)|^2$ in correspondence with expression (2).

phase matching is enhanced with the deviation from the optical transition line centre, which leads to the fall of the photon echo emission efficiency. Besides that, since the matching violation is different for different spectral components of the studied light, the arising disbalance also leads to the reduction of accuracy of broadband light field recovery. To solve this

problem, we analyse below the ways of suppressing the spectral dispersion, considering the natural shape of inhomogeneously broadened optical transition lines in real crystals.

3. Influence of dispersion effects

In the backward scheme, the AFC protocol is implemented in three stages in analogy with the initial scheme of the CRIB protocol [3, 12, 14]. First, the pulse of the signal light field is absorbed by the atoms in the crystal, which is accompanied by excitation of polarisation waves $\exp[-i(\omega t - \boldsymbol{k}_p \boldsymbol{r})]$ with the wave vectors $\boldsymbol{k}_p = [(\omega/c) + \delta k]\boldsymbol{e}_z$. Here $\delta k = \omega_0 \chi(\Delta)/2c$ is the additional change of the wave vector, caused by the interaction of light with resonance atoms; ω_0 is the centre frequency of the absorption line; $\Delta = \omega - \omega_0$ is the frequency detuning; and $\chi = \chi' + i\chi''$ is the susceptibility [$\omega_0\chi''/c = \alpha$ determines the coefficient of resonance absorption, and $\chi'(\Delta)$ characterises the anomalous dispersion in the course of resonance wave propagation].

The anomalous dispersion in the case of high optical density ($\alpha_0 L > 1$) can lead to the appearance of a supraluminal apparent group velocity or negative group velocity v in the propagation of the light pulse [35]. After the light absorption the excited atomic polarisation (coherence) is transferred to the long-living electron spin coherence by the action of the first controlling laser pulse. This gives rise to spin waves, possessing the wave vectors $\boldsymbol{k}_p - \boldsymbol{k}_1$ ($\boldsymbol{k}_1$ being the wave vector of the laser field) and conserving the information about the anomalous spectral dispersion in the signal light pulse propagation. It is important that the lifetime of the spin quantum coherence can be increased to a few hours in the system of rare-earth ions, using the reversible transfer of electronic coherence to the long-lived nuclear spin coherence [36].

At the third stage the second controlling laser pulse with a wave vector $\boldsymbol{k}_2$ restores the waves of atomic optical polarisation $\exp[-i(\omega t - \boldsymbol{k}_{ret}\boldsymbol{r})]$ with a new wave vector $\boldsymbol{k}_{ret} = \boldsymbol{k}_p - \boldsymbol{k}_1 + \boldsymbol{k}_2$. The automatic phasing of polarisation waves that follows can lead to the emission of the echo signal in analogy with the direct AFC protocol scheme, but in the opposite direction, if the wave vectors of the laser pulses are chosen as $\boldsymbol{k}_1 = \boldsymbol{e}_z\omega/c$ and $\boldsymbol{k}_2 = -\boldsymbol{e}_z\omega/c$. In this case, the wave vector of the phased polarisation waves is $\boldsymbol{k}_{ret} = (-\omega/c + \delta k)\boldsymbol{e}_z \approx -[\omega_0/c + \Delta(1/c + 1/v)]\boldsymbol{e}_z$. The phase and group velocity of these waves of polarisation are codirected with the light waves of the backward AFC echo signal, in contrast to the situation that takes place in the absorption of the signal light pulse.

It is known that in an optically thin medium the deviation from the phase matching condition affects the amplitude of the emitted light field E according to the formula $\sin((k_{ret} - k_p)L/2)/[(k_{ret} - k_p)L/2]$, and the radiation is intense only if $(k_{ret} - k_p)L = 1$ [37]. The high-efficiency restoration of the recorded information requires sufficiently precise fulfilment of the phase matching condition for all spectral components of the emitted field. The echo light field $A_{echo}(t, z)$ for the backward AFC scheme is expressed in terms of the Fourier integral over the spectrum of the signal field $A_s(\omega)$ at the crystal entrance:

$$A_{echo}(t, z) = \kappa\left(\frac{2\pi}{\Delta}\right)\int_{-\infty}^{\infty}\frac{1}{2\pi}\Gamma(\omega)\,e^{-i\omega(t - z/c)}A_s(\omega)\,d\omega, \qquad (2)$$

where $\Gamma(\omega) = \{1 - \exp[i\omega_0\chi(\omega)L/c]\}/[1 - i\chi'(\omega)/\chi''(\omega)]$ is the spectral characteristic (SC) of the memory; χ' is the refractive index of the crystal with the AFC structure; $\alpha = 2(\omega_0/c)\chi'' = \alpha_0/f$ is the averaged absorption coefficient of the crystal; and $2\pi\kappa/\Delta$ is the factor that determines the presence of irreversible damping of polarisation during the time $2\pi/\Delta$, which is caused by the finite spectral width of the AFC structure [the Gaussian shape of the peak lines yields $\kappa = \exp(-3.5/f^2)$].

As seen from Eqn (2), the SC of the memory determines the spectral quantum efficiency of the AFC protocol according to $\eta(\omega) = |\Gamma(\omega)|^2$ at sufficiently high values of the finesse f and, correspondingly, $\kappa \approx 1$. It is important that the absorption coefficient α in the spectral region, where the recording of the signal light field occurs, is determined by the parameters of the resonance absorption lines, but the susceptibility $\chi \sim \chi'(\omega)$ depends also on the presence of the resonance lines in the vicinity, close to this frequency region. It is remarkable that according to relation (2), the influence of the spectral dispersion appears to be insignificant both in the case of a sufficiently small value of the frequency dispersion [$\chi'(\omega)/\chi''(\omega) = 1$), and in the case of a small optical density of the atomic transition [$\alpha(\omega)L < 1$]. In this case, expanding the function $\Gamma(\omega)$ into a series in powers of the small parameter $\omega_0\chi(\omega)L/c \ll 1$ we find that the quantum efficiency $\eta(\omega) \approx (\alpha(\omega)L)^2/4 \ll 1$, which agrees with the experimental results of Refs [27–29, 38–40].

To demonstrate the strong influence of the spectral dispersion on the quantum efficiency, Figs 3 and 4 present the plots of the spectral efficiency $\eta(\omega)$ for two cases. In the first case, the AFC structure covers all inhomogeneous broadening of the optical transition sine [16], having the typical shape of a Gaussian line with the width Δ_{in} [41]; the spectral width of the AFC structure significantly exceeds the spectral width of the light pulses. In the second limit case it is assumed that the AFC structure is formed in a narrow part of the inhomogeneous width ($\Delta_0 \ll \Delta_{in}$). Figures 3 and 4 present the spectral dependences of the quantum efficiency both neglecting the spectral dispersion effects and considering them. The plots obtained by numerical calculations show that the spectral dispersion in optically dense media strongly reduces the spectral width, within which the extremely high quantum efficiency can be implemented. Thus, from the comparison of Figs 3a and 4a with Figs 3b and 4b one can see that with the spectral dispersion taken into account the quantum efficiency specified by the relation $\eta(\omega) > \eta_0$ exists only within a narrow spectral region. The width of this region does not essentially change after achieving a certain value of the optical density that corresponds to the given quantum efficiency η_0 and the finesse f of the lines in the AFC structure.

The character of the spectral quantum efficiency behaviour is explained by the fact that at a sufficiently high optical density ($\alpha_0 L \gg 1$) the spectral quantum efficiency is defined as $\eta(\omega) = |1 - i\chi'(\omega)/\chi''(\omega)|^{-2}$, the spectral bandwidth Δ_{qm} of the high quantum efficiency being independent of αL. For example, for the AFC structure excited inside the entire inhomogeneous broadening contour of the Gaussian type, we have $\eta(\omega) = \eta_G(\omega) = |1 - i(\omega/|\omega|)\mathrm{erfi}(\omega/\sqrt{2}\,\Delta_{in})|^{-2}$. Thus, the maximal achievable spectral width Δ_{qm} depends only on the inhomogeneous broadening line shape.

To increase the spectral width Δ_{qm} essentially, let us consider the version, in which the AFC structure is created in a certain specified spectral interval $\Delta_0 < \Delta_{in}$. As shown below, the optimal choice of the value of Δ_0 can significantly increase the spectral interval Δ_{qm}.

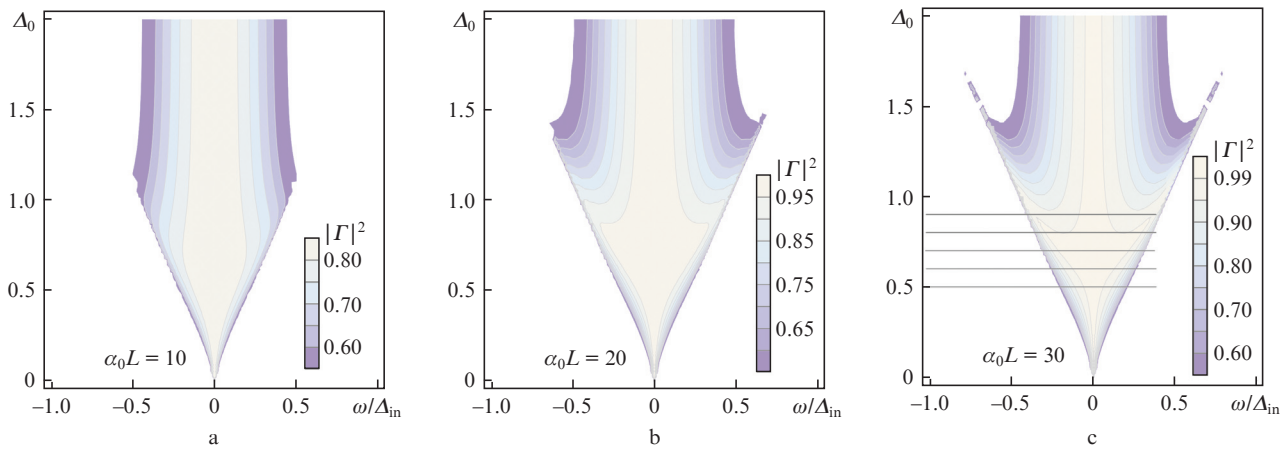

Figure 5. Calculated spectral efficiency $\eta(\omega)$ vs. the width of the spectral interval Δ_0 (in the units of Δ_{in}) for the optical density $\alpha_0 L =$ (a) 10, (b) 20 and (c) 30.

4. Optimal parameters of high spectral quantum efficiency

In correspondence with the abovementioned result, the quantum efficiency decreases with increasing frequency detuning at a high optical density ($\alpha_0 L \gg 1$). To solve this problem, we performed numerical simulation of the echo emission efficiency in the modified AFC structure.

Figure 5 presents the calculated spectral efficiency $\eta(\omega)$ versus the spectral interval Δ_0 (in the units of Δ_{in}) for three different values of the initial optical density $\alpha_0 L = 10$, 20 and 30. In the case of a relatively small optical density ($\alpha_0 L = 10$), we can see an increase in the spectral region of high quantum efficiency for $\Delta_0 \approx 0.65$. In this case, $\eta(\omega) > 0.8$ in the frequency region $|\omega| < 0.2\Delta_{in}$ ($\Delta_{qm} = 0.4\Delta_{in}$).

In the second case ($\alpha_0 L = 20$), one can see even a greater increase in the spectrum width, within which the high quantum efficiency area acquires the shape of an arrow in the plane $(\Delta_0, \omega/\Delta_{in})$, where $\eta(\omega) > 0.95$ is valid for $\Delta_0 \approx 0.85\Delta_{in}$ in the maximal frequency interval $\Delta_{qm} = 0.6\Delta_{in}$ ($|\omega| < 0.3\Delta_{in}$). For example, for the $Pr^{3+}:Y_2SiO_5$ crystal with $\Delta_{in} =$ 5 GHz and $\alpha = 23$ cm^{-1} for the quantum efficiency $\eta(\omega) >$ 0.95 the width of the spectrum is $\Delta_0 = 0.85\Delta_{in} = 4.25$ GHz, the crystal length being 0.87 cm.

In the third case (Fig. 5c), we have the highest quantum efficiency, particularly necessary for quantum computer memory. This situation arises at the optical density $\alpha_0 L = 30$. The region of the maximal quantum efficiency in the plane $(\Delta_0, \omega/\Delta_{in})$ has the shape of a sharpened anchor. Under these conditions, the quantum efficiency $\eta(\omega) > 0.99$ is possible for the frequency comb with the width $\Delta_0 \approx 0.8\Delta_{in}$ in the same frequency region $|\omega| < 0.3\Delta_{in}$ with the width $\Delta_{qm} = 0.6\Delta_{in}$. The spectral behaviour of the quantum efficiency for $\alpha_0 L =$ 30 near the optimal value of the spectral width Δ_{qm} is discussed below in more detail, using the numerical data, presented in Fig. 6 for the spectral widths of the AFC structure $\Delta_0 = 0.5, 0.6, 0.7, 0.8$ and 0.9 (in the units of Δ_{in}).

As seen from the Figure, for $\alpha_0 L = 30$ the increase in Δ_0 from $0.5\Delta_{in}$ to $0.6\Delta_{in}$ and further to $0.7\Delta_{in}$ leads to the growth of the spectral width of the high quantum efficiency region. For $\Delta_0 = 0.7\Delta_{in}$ the quantum efficiency is close to 100% [$\eta(\omega) \geqslant 0.999$] within the spectral range from $-0.2\Delta_{in}$ to $0.2\Delta_{in}$. Further increase in the spectral width of the AFC structure to $\Delta_0 = 0.8\Delta_{in}$ is accompanied by the growth of the spectral width of the high quantum efficiency region [where $\eta(\omega) \geqslant 0.99$], but in this case two local minima at the frequencies $\omega = \pm 0.2\Delta_{in}$ appear, in which $\eta(\pm 0.2\Delta_{in}) = 0.99$. The depth of the minima increases with increasing AFC structure width. In Fig. 6 it is also seen that at $\Delta_0 = 0.9\Delta_{in}$ the depth of the minima corresponds to $\eta = 0.96$ at $\omega \approx \pm 0.25\Delta_{in}$, and then η is restored only to 0.99 at $\omega \approx \pm 0.35\Delta_{in}$. Further increase in the spectral width ($\Delta_0 > 0.9\Delta_{in}$) leads to even greater narrowing of the frequency range, where the implementation of high quantum efficiency is possible.

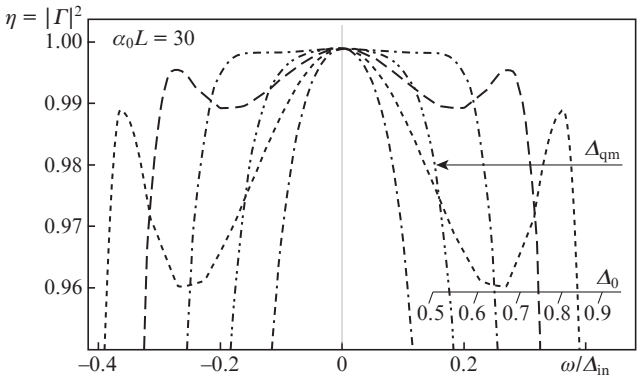

Figure 6. Spectral efficiency $\eta(\omega)$ for the optical density $\alpha_0 L = 30$ and $\Delta_{qm} = 0.6\Delta_{in}$ vs. ω/Δ_{in} (the sections marked by lines in Fig. 5); the arrow shows the quantum efficiency behaviour at $\Delta_0 = 0.6\Delta_{in}$.

Thus, to achieve the desired quantum efficiency of the memory, e.g., $\eta(\omega) \geqslant 0.99$, the most optimal way is to create an AFC structure in the spectral range $\Delta_0 = 0.8\Delta_{in}$. In this case, the given quantum efficiency is implemented in the spectral range $\Delta_{qm} = 0.6\Delta_{in}$. To achieve the superefficient quantum memory with $\eta(\omega) \geqslant 0.999$, it is necessary to have $\alpha_0 L \geqslant$ 30 and $\Delta_0 = 0.7\Delta_{in}$. Note that the memory cells with high quantum efficiency allow the application of the error correction procedure and, therefore, can be used in a quantum com-

puter. Ultrahigh quantum efficiency for broadband light fields is also possible using the AFC structure in a cavity [42], although in a narrower spectral range. Experimental achievement of the optical density $\alpha_0 L = 30$ requires either growing a crystal of larger size, or placing the atoms in a waveguide structure, in which a significant increase in the atom-field coupling constant is possible [43]. However, in the latter case the modernisation of the scheme is required, since the amplitude of light fields can become essentially inhomogeneous in space, which complicates exact control of the optical coherence using external laser fields.

5. Conclusions

As shown in Ref. [32], the absence of exact reversibility in the AFC protocol scheme [15] leads to negative dispersion effects in the emission of the echo signal in optically dense media, which reduces the quantum efficiency and the accuracy of the initial signal field recovery. In the present paper, possible implementations of the modified AFC protocol (MAFC) are analysed in detail, in which the zero spectral dispersion is provided in the operation range of the MAFC structure. Based on the performed numerical calculations, we demonstrated the characteristic features of the spectral behaviour of the quantum efficiency depending on the characteristic parameters of the optical transition and the spectral width of the created AFC structure. The analysis of the numerical calculations has shown that for the implementation of the ~95% quantum efficiency the required optical density is $\alpha_0 L = 20$, which is possible in the $Pr^{3+}:Y_2SiO_5$ crystal [7] having a length 0.87 cm and a coefficient of resonance absorption $\alpha = 23$ cm^{-1}. The achievement of a higher spectral quantum efficiency (above 99%) in the same spectral interval will be possible for the optical density $\alpha_0 L = 30$. Finally, the implementation of ultrahigh quantum efficiency (above 99%) is possible in a crystal with an optical density $\alpha_0 L = 30$, but in a narrower spectral range $\Delta_{qm} = 0.4\Delta_{in}$. Note that the optical density required in this case can be achieved, e.g., using photonic crystal waveguides, where the interaction of light with resonance atoms can be additionally enhanced by more than an order of magnitude [43]. At the same time, strong spatial localisation of light in the transverse plane of the waveguide gives rise to new problems in the implementation of high-accuracy control of optical coherence, which will require further improvement of the MAFC protocol, e.g., by using Raman atomic transitions [44]. This is a subject of further studies.

Acknowledgements. The work was supported by the Russian Science Foundation (Grant No. 14-12-01333P).

References

1. Hahn E.L. *Phys. Rev.*, **80**, 580 (1950).
2. Kurnit N.A., Abella I.D., Hartmann S.R. *Phys. Rev. Lett.*, **13**, 567 (1964).
3. Moiseev S.A., Kröll S. *Phys. Rev. Lett.*, **87**, 173601 (2001).
4. Tittel W., Afzelius M., Chaneliére T., Cone R., Kröll S., Moiseev S.A., Sellars M. *Laser Photon. Rev.*, **267**, 244 (2010).
5. Usmani I., Afzelius M., de Riedmatten H., Gisin N. *Nat. Commun.*, **1**, 12 (2010).
6. Bonarota M., Le Gouët J.-L.L., Chanelière T. *New J. Phys.*, **13**, 013013 (2011).
7. Gündoğan M., Mazzera M., Ledingham P.M., Cristiani M., De Riedmatten H. *New J. Phys.*, **15**, 045012 (2013).
8. Sinclair N., Saglamyurek E., Mallahzadeh H., Slater J.A., George M., Ricken R., Hedges M.P., Oblak D., Simon C., Sohler W., Tittel W. *Phys. Rev. Lett.*, **113**, 053603 (2014).
9. Saglamyurek E., Grimau Puigibert M., Zhou Q., Giner L., Marsili F., Verma V.B., Woo Nam S., Oesterling L., Nippa D., Oblak D., Tittel W. *Nat. Commun.*, **7**, 11202 (2016).
10. Sangouard N., Simon C., De Riedmatten H., Gisin N. *Rev. Mod. Phys.*, **83**, 33 (2011).
11. Pérez-Delgado C.A., Kok P. *Phys. Rev. A*, **83**, 012303 (2011).
12. Moiseev S.A., Noskov M.I. *Laser Phys. Lett.*, **1** (6), 303 (2004).
13. Kraus B., Tittel W., Gisin N., Nilsson M., Kröll S., Cirac J. *Phys. Rev. A*, **73**, 020302 (2006).
14. Moiseev S.A., Tittel W. *Phys. Rev. A*, **82**, 012309 (2010).
15. De Riedmatten H., Afzelius M., Staudt M.U., Simon C., Gisin N., Riedmatten H.D. *Nature*, **456**, 773 (2008).
16. Afzelius M., Simon C., De Riedmatten H., Gisin N. *Phys. Rev. A*, **79**, 052329 (2009).
17. Alexander A.L., Longdell J.J., Sellars M.J., Manson N.B. *Phys. Rev. Lett.*, **96**, 043602 (2006).
18. Hétet G., Longdell J.J., Alexander A.L., Lam P.K., Sellars M.J. *Phys. Rev. Lett.*, **100**, 023601 (2008).
19. Moiseev S.A., Arslanov N.M. *Phys. Rev. A*, **78**, 023803 (2008).
20. Damon V., Bonarota M., Louchet-Chauvet A., Chanelière T., Le Gouët J.L. *New J. Phys.*, **13**, 093031 (2011).
21. Moiseev S.A. *Phys. Rev. A*, **83**, 012307 (2011).
22. McAuslan D.L., Ledingham P.M., Naylor W.R., Beavan S.E., Hedges M.P., Sellars M.J., Longdell J.J. *Phys. Rev. A*, **84**, 022309 (2011).
23. Grezes C., Julsgaard B., Kubo Y., Stern M., Umeda T., Isoya J., Sumiya H., Abe H., Onoda S., Ohshima T., Jacques V., Esteve J., Vion D., Esteve D., Mølmer K., Bertet P. *Phys. Rev. X*, **4**, 1 (2014).
24. Grezes C., Kubo Y., Julsgaard B., Umeda T., Isoya J., Sumiya H., Abe H., Onoda S., Ohshima T., Nakamura K., Diniz I., Auffeves A., Jacques V., Roch J.-F., Vion D., Esteve D., Mølmer K., Bertet P. *Comptes Rendus Phys.*, **17**, 693 (2016).
25. Saglamyurek E., Sinclair N., Jin J., Slater J.A., Oblak D., Tittel W., Bussieres F., George M., Ricken R., Sohler W. *Nature*, **469**, 512 (2011).
26. Sun Y., Thiel C.W., Cone R.L. *Phys. Rev. B*, **85**, 165106 (2012).
27. Amari A., Walther A., Sabooni M., Huang M., Krll S., Afzelius M., Usmani I., Lauritzen B., Sangouard N., De Riedmatten H., Gisin N. *J. Lumin.*, **130**, 1579 (2010).
28. Zhou Z.-Q., Wang J., Li C.-F., Guo G.-C. *Sci. Rep.*, **3**, 2754 (2013).
29. Cho Y.-W., Campbell G.T., Everett J.L., Bernu J., Higginbottom D.B., Cao M.T., Geng J., Robins N.P., Lam P.K., Buchler B.C. *Optica*, **3**, 100 (2016).
30. Sabooni M., Li Q., Kröll S., Rippe L. *Phys. Rev. Lett.*, **110**, 133604 (2013).
31. Sabooni M., Kometa S.T., Thuresson A., Kröll S., Rippe L. *New J. Phys.*, **15**, 035025 (2013).
32. Moiseev S.A., Le Gouët J.-L. *J. Phys. B*, **45**, 124003 (2012).
33. Chebotaev V.P., Dubetskii B.Y. *Appl. Phys. B: Photophys. Laser Chem.*, **31**, 45 (1983).
34. Dubetskii B.Y., Chebotaev V.P. *JETP Lett.*, **41**, 328 (1985) [*Pis'ma Zh. Exp. Teor. Fiz.*, **41**, 267 (1985)].
35. Wang L., Kuzmich A., Dogariu A. *Nature*, **406**, 277 (2000).
36. Zhong M., Hedges M.P., Ahlefeldt R.L., Bartholomew J.G., Beavan S.E., Wittig S.M., Longdell J.J., Sellars M.J. *Nature*, **517**, 177 (2015).
37. Boyd R.W. *Nonlinear Optics* (San Diego: Acad. Press, 2008) p. 640.
38. Gündoğan M., Ledingham P.M., Almasi A., Cristiani M., De Riedmatten H. *Phys. Rev. Lett.*, **108**, 190504 (2012).
39. Clausen C., Usmani I., Bussieres F., Sangouard N., Afzelius M., De Riedmatten H., Gisin N., Bussières F. *Nature*, **469**, 508 (2011).

40. Usmani I., Clausen C., Bussières F., Sangouard N., Afzelius M., Gisin N. *Nat. Photonics*, **6**, 234 (2012).
41. Allen L., Eberly J.H. *Optical Resonance and Two-Level Atoms* (New York: John Wiley & Sons, Inc., 1975; Moscow: Mir, 1978).
42. Perminov N.S., Moiseev S.A. arXiv:1706.00592 (2017).
43. Yuan, C., Zhang W., Huang Y., Peng J. *Eur. Phys. J. D*, **70**, 185 (2016).
44. Moiseev S.A., Tittel W. *New J. Phys.*, **13**, 063035 (2011).